NTUTH 9012
oct. '90

NTU-TH-90-12

FIELD THEORY ON THE RANDOM BLOCK LATTICE†

FERMILAB
DEC 26 1990
LIBRARY

T.W. CHIU

Department of Physics, National Taiwan University, Taipei, Taiwan 10764, Republic of China.

Abstract

Field theories are formulated on the random block lattice in which the sites are cartesian product of D sets of random coordinates, one from each dimension, where D is the dimension of the space-time. The gauge field, the scalar field, the fermion field and the vacuum polarization in QED are studied respectively.

INTRODUCTION

A random-block lattice[1,2] (RBL) in D dimensional Euclidean space is constructed by Cartesian product of D sets of random coordinates, one from each dimension. Each set of random coordinates are presumably randomly distributed on an interval $[0, L]$ with uniform probability. The separation between any two neighbouring coordinates in each dimension thus obeys the Poisson distribution. It is of course possible to impose other probability distributions. However I always refer RBL to those obey the Poisson distribution. An example of a 2-dimensional RBL is shown in Fig. 1 of Ref. 2. My motivations of formulating field theories on RBL are essentially : (i) RBL as an alternative regularization scheme, (ii) to circumvent the difficulties such as the fermion doubling problem on a regular lattice, (iii) physical observables averaged over a large number of RBLs can manifest rotational and translational symmetry and (iv) field theoretic calculations on a random-block lattice are much easier than their counterparts on a random lattice[3]. In this talk, I review the present status of field theories on RBL and discuss further investigations.

GAUGE FIELD[4]

On a 4-d RBL, the link variable pointing from the site i to the site $i+\mu$ is

$$U_\mu(i) = \exp[igl_i^\mu A_\mu(x_i + \frac{l_i^\mu}{2})]$$

where $l_i^\mu = x_{i+\mu} - x_i$. The action of the $SU(N)$ pure gauge theory is

$$A = \beta \sum_p w_p[1 - \frac{1}{N} Re(trU_p)] \equiv \beta E$$

where U_p is the ordered product of the link variables around the plaquette p, $\beta = 2N/g^2$ and w_p is the weight of the plaquette p, which is the ratio of the area dual to p and the area of p,

$$\begin{aligned} w_p &= \frac{\widetilde{A}_p}{A_p} \\ A_p &= l_i^\mu l_i^\nu \\ \widetilde{A}_p A_p &= l_i^{(1)} l_i^{(2)} l_i^{(3)} l_i^{(4)} \end{aligned}$$

In the continuum limit, this action goes to the continuum gauge field action

$$A_C = \int d^4x \, \frac{1}{4} F^a_{\mu\nu} F^a_{\mu\nu}$$

If $O(U)$ is a function of the link variables U, then its quantum expectation value is

$$< O >= \frac{1}{V^{N_s}} \int \prod_{i=1}^{N_s} d^4x_i \frac{\int \prod_{l=1}^{N_l} dU_l O(U) e^{-A(U)}}{\int \prod_{l=1}^{N_l} dU_l e^{-A(U)}}$$

where N_s is the number of sites, $N_l = 4N_s$ is the number of links, $N_p = 6N_s$ is the number of plaquettes and V is the volume of the lattice. The observables calculated in Ref. 4 are the average energy per plaquette and its derivative, specific heat. The results are similar to their counterparts on a regular lattice, except the crossovers from strong to weak coupling regimes in $SU(2)$ and $SU(3)$ are more smooth on a RBL than on a regular lattice.

SCALAR FIELD

The action of real scalar field on a 4-d RBL can be written as

$$A_L = \frac{1}{2} \sum_i \sum_\mu \lambda_{i\mu} (\phi_i - \phi_{i+\mu})^2 + \frac{1}{2} m^2 \sum_i \omega_i \phi_i^2 \equiv \tilde{\Phi} M \Phi \tag{1}$$

† invited talk at the 25th International Conference on High Energy Physics, Singapore, August, 1990.

RETURN TO
NAME
ROUTE TO

where ϕ_i is the real scalar field at the site i, $\lambda_{i\mu}$ is the link weight of the link $(i, i+\mu)$

$$\lambda_{i\mu} = (l_i^\mu)^{-1} \prod_{\nu \neq \mu} \frac{(x_{i+\nu} - x_{i-\nu})}{2} \tag{2}$$

and ω_i is the weight at the site i,

$$\omega_i = \prod_\mu \frac{(x_{i+\mu} - x_{i-\mu})}{2} \tag{3}$$

In the continuum limit the lattice action goes to

$$A_c = \int d^4x \frac{1}{2}[\partial_\mu \phi \partial^\mu \phi + m^2 \phi^2]$$

The two-point Green's function, scalar propagator is

$$S(x) = \frac{1}{V^{N_s-2}} \int \prod_{i=1}^{N_s} d^4y_i \prod_{j=1}^{2} \delta^4(y_j - x_j) S^L(y_1, y_2) \tag{4}$$

where $x_\mu = (x_1 - x_2)_\mu$ and

$$S^L(y_1, y_2) = < \phi_{y_1} \phi_{y_2} > = (M^{-1})_{y_1 y_2}. \tag{5}$$

In Fig. 1 , the massless scalar propagator is denoted by crosses which are calculated using 1000 of 20^4 RBLs with antiperiodic boundary conditions. The result is quite independent of the actual location of the two end points. This implies that the translational and rotational invariance manifest after ensemble averaging over a large number of RBLs. It is compared to the continuum solution $S_c(x) = 1/4\pi^2 x^2$ which is plotted as the solid line and the regular lattice propagator which is denoted by squares. The scalar propagator in RBL agrees very well with the continuum solution at large distances ($x > 1$).

The scalar propagator in momentum space can be obtained by the following Fourier transformation

$$\tilde{S}(p) = \frac{1}{V^{N_s}} \int \prod_{k=1}^{N_s} d^4x_k \frac{1}{V} \sum_i \sum_j \omega_i \omega_j \, e^{ip\cdot(x_i - x_j)} S^L(x_i, x_j)$$

where $S^L(x_i, x_j)$ is given in eq.(5). In Fig. 2, the massless scalar propagator in momentum space is denoted by crosses which are calculated using 1000 of 20^4 RBLs with antiperiodic boundary conditions. The continuum propagator $\tilde{S}^c(p) = (p^2)^{-1}$ is plotted as the solid line and the regular lattice propagator $\tilde{S}^R(p) = [4 \sum_\mu sin^2(p_\mu a/2)]^{-1}$ is denoted by squares. The scalar propagator on RBL agrees with the continuum solution for all momentum values except the

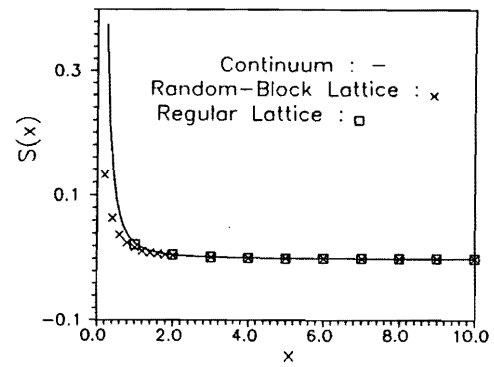

Figure 1: Massless scalar propagator in position space.

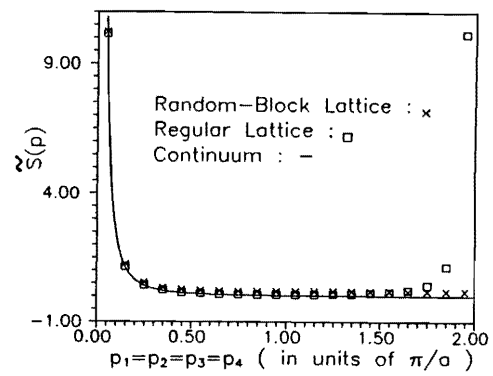

Figure 2: Massless scalar propagator in momentum space.

small deviations at very large momenta. On the other hand, the regular lattice propagator must be in complete disagreement with the continuum propagator in the vicinity of $p_i = 2n\pi/a, n = 1, 2, 3, ...$ due to periodicity.

FERMION FIELD[2,5,6]

The action of Dirac fermion field on RBL can be written as

$$\begin{aligned} A_L &= \sum_i \sum_\mu \omega_i K_i^\mu \bar{\psi}_i \gamma^\mu [\psi_{i+\mu} - \psi_{i-\mu}] + m \sum_i \omega_i \bar{\psi}_i \psi_i \\ &\equiv \bar{\Psi}[\gamma^\mu T^\mu + mW]\Psi \end{aligned}$$

where ψ_i and $\bar{\psi}_i$ are two independent 4-component spinors at site i, ω_i is the weight at site i, K_i^μ is the inverse of the distance between the sites $i+\mu$ and $i-\mu$, $K_i^\mu = (x_{i+\mu} - x_{i-\mu})^{-1}$, m is the mass and γ_μ are the Dirac matrices. In the continuum limit, it

goes to the continuum Dirac fermion action

$$A_c = \int d^4x \bar{\psi}(x)(\gamma_\mu \partial_\mu + m)\psi(x)$$

The two-point Green's function, fermion propagator is

$$\begin{aligned} S_F(x) &\equiv S_0(x) + \gamma_\mu S_\mu(x) \\ &= \frac{1}{V^{N_s-2}} \int \prod_{i=1}^{N_s} d^4y_i \prod_{j=1}^{2} \delta^4(y_j - x_j) S_F^L(y_1, y_2) \end{aligned}$$

where $x_\mu = (x_1 - x_2)_\mu$ and

$$\begin{aligned} S_F^L(y_1, y_2) &\equiv [S_0^L]_{y_1 y_2} + \gamma_\mu [S_\mu^L]_{y_1 y_2} \qquad (6) \\ &= < \psi_{y_1} \bar{\psi}_{y_2} > = [\gamma_\mu T_\mu + mW]^{-1}_{y_1 y_2} \\ &= [W^{-1/2}(m - \gamma_\mu T'_\mu)(m^2 - (T')^2)^{-1} W^{-1/2}]_{y_1 y_2} \end{aligned}$$

where $T'_\mu = W^{-1/2} T_\mu W^{-1/2}$; while for the massless fermion,

$$\begin{aligned} S_F^L(y_1, y_2) &= < \psi_{y_1} \bar{\psi}_{y_2} > = \gamma_\mu (T_\mu)^{-1}_{y_1 y_2} \\ &= \gamma_\mu [(T_\mu)(T^2)^{-1}]_{y_1 y_2} \equiv \gamma_\mu (S_\mu^L)_{y_1 y_2} \qquad (7) \end{aligned}$$

Results of fermion propagators in position space has been described in Ref. 2, 5 and 6. In summary, the fermion propagator on RBL agrees very well with the continuum propagator for distances greater than three average lattice spacings. In the continuum limit $a \to 0$, the discrepancies at small distances ($x < 3a$) goes to zero. This can be shown explicitly by increasing the number of sites in every dimension while keeping the volume fixed[6].

The fermion propagator in momentum space can be obtained by the following Fourier transformation

$$\tilde{S}_F(p) \equiv \tilde{S}_0(p) + i\gamma_\mu \tilde{S}_\mu(p)$$

$$= \frac{1}{V^{N_s}} \int \prod_{k=1}^{N_s} d^4x_k \frac{1}{V} \sum_i \sum_j \omega_i \omega_j e^{ip\cdot(x_i - x_j)} S_F^L(x_i, x_j)$$

For the massless fermion, only the vector components $\tilde{S}_\mu(p)$ survive. In Fig. 3, the massless fermion propagator in momentum space is denoted by crosses which are calculated using 1000 of 10^4 RBLs with antiperiodic boundary conditions. For the convenience of displaying results, I have chosen symmetric momentum ($p_1 = p_2 = p_3 = p_4$) so that $\tilde{S}_\mu(p)$ turns out to be almost the same for all μ. The continuum propagator $\tilde{S}_F^c(p) = i\gamma_\mu p_\mu / p^2$ is plotted as the solid line and the regular lattice propagator $\tilde{S}_F^R(p) = i\gamma_\mu a sin(p_\mu a)/[\sum_\mu sin^2(p_\mu a)]$ is plotted as dashed lines. The fermion propagator on

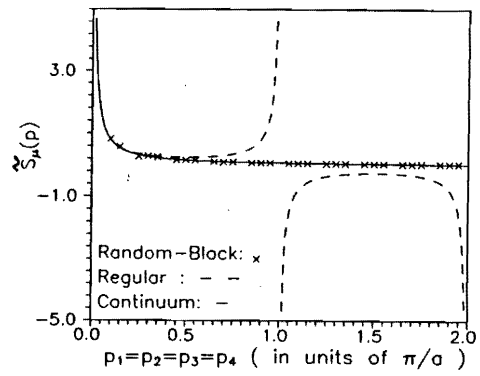

Figure 3: Massless fermion propagator in momentum space.

RBL agrees with the continuum solution for all momentum values, while the regular lattice propagator is in complete disagreement with the continuum propagator except in the vicinity of small momenta. One of the 15 doubled modes of the regular lattice propagator at $(\frac{\pi}{a}, \frac{\pi}{a}, \frac{\pi}{a}, \frac{\pi}{a})$ is shown explicitly. The propagator of a left(right)-handed Weyl fermion is $\tilde{S}_{L,R}(p) = \tilde{S}_4(p) \pm i \sum_{j=1}^{3} \sigma_j \tilde{S}_j(p)$ where $\sigma_j, j = 1, 2, 3$ are the Pauli matrices. Therefore Fig. 3 also demonstrates that a single species of Weyl fermion is possible on the 4-d random-block lattice.

VACUUM POLARIZATION[6]

The vacuum polarization tensor is one of the most important quantity to study since the number of species of fermion must appears as a numerical factor of it, and thus provides a good test for any scheme of lattice fermion. Elimination of spectrum doubling in the free field limit does not gaurantee the same would hold in weak coupling perturbation theory.

The action of QED on a 4-d RBL can be written as

$$A_L = \sum_i \sum_\mu \omega_i K_i^\mu [\bar{\psi}_i \gamma_\mu U_\mu(i) \psi_{i+\mu} - \bar{\psi}_i \gamma_\mu U_\mu^+(i-\mu) \psi_{i-\mu}]$$

$$+ m \sum_i \omega_i \bar{\psi}_i \psi_i + \beta \sum_p w_p [1 - Re(U_p)]$$

where $\beta = 1/e^2$ and other symbols have defined before. In the continuum limit, it goes to the continuum QED action

$$A_c = \int d^4x [\bar{\psi}(x) \gamma_\mu (\partial_\mu + igA_\mu + m) \psi(x) + \frac{1}{4} F_{\mu\nu} F_{\mu\nu}].$$

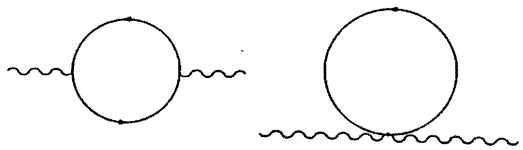

Figure 4: The Feynman diagrams contributing to the lowest order vacuum polarization tensor on the lattice. Diagram (b) does not exist in the continuum theory.

In the weak gauge coupling limit, the lattice action can be expanded in the order of g to yield the Feynman rules on the random-block lattice. The vacuum polarization tensor which consists of two parts corresponding to Fig. 4a and Fig. 4b respectively.

In position space the seagull term Fig. 4b vanishes except at $x \equiv |x_i - x_j| = 0$. For $x > 0$, only the Fig. 4a contributes to the vacuum polarization tensor and it is

$$
\begin{aligned}
& {}^{(a)}\Pi^L_{\mu\nu}[x_i + \frac{l_i^\mu}{2}, x_j + \frac{l_j^\nu}{2}] \\
\simeq\ & [\, Tr(\gamma_\mu (S_F^L)_{i+\mu,j} \gamma_\nu (S_F^L)_{j+\nu,i}) \\
+\ & Tr(\gamma_\mu (S_F^L)_{i+\mu,j+\nu} \gamma_\nu (S_F^L)_{j,i}) \\
+\ & Tr(\gamma_\mu (S_F^L)_{i,j} \gamma_\nu (S_F^L)_{j+\nu,i+\mu}) \\
+\ & Tr(\gamma_\mu (S_F^L)_{i,j+\nu} \gamma_\nu (S_F^L)_{j,i+\mu}) + (\mu \leftrightarrow \nu)]
\end{aligned}
$$

where S_F^L is the fermion propagator defined in eq.(6) or eq.(7). For symmetric configurations (end points on body diagonal $x_1 = x_2 = x_3 = x_4$), in continuum QED, all diagonal components $\Pi^c_{\mu\mu}$ are equal, and all off-diagonal components $\Pi^c_{\mu\nu} (\mu \neq \nu)$ are equal. For the massless fermion, the off-diagonal components only have a sign difference from the diagonal components. In Fig. 5, components of $\Pi_{\mu\nu}$ of massless QED are calculated using 1024 RBLs, each of 20^4 sites and with periodic boundary conditions. The average lattice spacing is $a = 1.0$. The end points are lying on the body diagonal. For point-splitting equal to zero, the results are almost 10 to 16 times of the corresponding values in the continuum QED. The difference is mainly due to the presence of the 15 species of pseudovectors, arising from the chiral symmetry breaking of the doubled modes[2]. The effects of these pseudovectors can be suppressed by splitting the end-points at the interaction vertices. For example, the end-points $i \equiv (x_1, x_2, x_3, x_4)$ and $j \equiv (y_1, y_2, y_3, y_4)$ of the forward-moving propagator, are split from the end-points $i' \equiv (x_1 - \varepsilon, x_2 + \varepsilon, x_3 - \varepsilon, x_4 + \varepsilon)$ and $j' \equiv (y_1 - \varepsilon, y_2 + \varepsilon, y_3 - \varepsilon, y_4 + \varepsilon)$ of the backward-moving propagator. The value of ε can be taken to be *any* fraction of the average lattice spacing a. The results are very insensitive to the ε value.

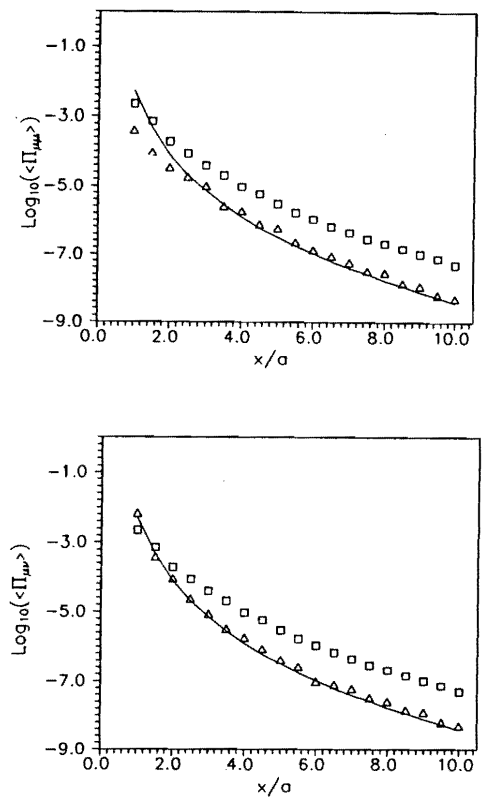

Figure. 5 Vacuum Polarization Tensor of massless QED in position space. The results with point-splitting $1.0a$ are denoted by triangles which are in agreement with the continuum QED (the solid line), while those without point-splitting are denoted by squares which are about 10 to 16 times larger than the continuum QED. (a) the average of the diagonal components $\Pi_{\mu\mu}$. (b) the average of the off-diagonal components $\Pi_{\mu\nu}, \mu \neq \nu$.

In Fig. 5, the ε value has been fixed to be $0.5a$. The average of the diagonal components of the point-split vacuum polarization tensor agrees very well with the continuum limit for distances greater than two average lattice spacings. In Fig. 5b, the average of the off-diagonal components of the point-split vacuum polarization tensor agrees very well with the continuum limit for all distances. This clearly shows

that the leading order contribution of the doubled modes to the vacuum polarization tensor transforms like a scalar, and thus only affects the diagonal components. It is well known that point-splitting at an interaction vertex would violate gauge invariance if the link variables are not taken into account properly. However in the weak coupling limit ($\beta \to \infty$), the link variables are almost frozen to one. Moreover we can always choose the temporal gauge and restrict the point splitting only in the time direction. Therefore it is plausible that the dynamical effects of link variables would not change the above results significantly. Nevertheless a dynamical calculation including gauge fields must be carried out in order to justify the above approximation.

CONCLUSION and DISCUSSION

In this talk, I have shown that random-block lattice provides an alternative gauge invariant regularization scheme for non-perturbative studies of field theories and avoids fermion doubling problem without explicitly breaking the chiral symmetry or introducing any non-local interactions. It has advantages over the regular lattice and the completely random lattice. The fermion doubling problem can be evaded on RBL by using an ensemble of RBLs and evaluating the path integrals on each one of the lattices, and finally taking the ensemble average. I believe that this is the right way of evaluating the path integral rather than just fixing it to a single (regular) lattice. Even in the case of scalar propagator in momentum space (Fig. 2), ensemble averaging yields results in good agreement with the continuum propagator up to very large momentum values while the regular lattice propagator is in complete disagreement with the continuum propagator in the vicinity of $p_i = 2n\pi/a, n = 1,2,3,...$ due to periodicity. This shows that physical observables averaged over a large number of RBLs can manifest rotational and translational symmetry.

The QCD scale parameter Λ is being calculated on RBL. This can be determined by measuring the heavy quark potential and the string tension. Another crucial task is to show that the axial anomaly does have the correct continuum limit. The calculations of the triangle diagrams on 4-D RBL are very time-consuming and are now in progress. At this moment, calculations of the standard model on RBL seem to be remote, though in principle are possible. Since the chiral fermion does not have a proper treatment on the regular lattice, the RBL could be a useful tool for nonperturbative calculations involving chiral fermions.

ACKNOWLEDGEMENT

This research was partially supported by National Science Council, Republic of China and US Department of Energy. I am grateful to Professor Geoffrey C. Fox for his very kind hospitality during my visit to CALTECH from August 1987 to August 1989. I also thank the Division of Physics, Mathematics and Astronomy at CALTECH for the kind hospitality extended to me during my visit.

REFERENCES

1. T.W. Chiu, " Fermion Spectrum on the Random Lattices ", contributed paper to the XXIII International Conference on High Energy Physics, Berkeley, 1986.
2. T.W. Chiu, Phys. Lett. B 206 (1988) 510.
3. N.H. Christ, R. Friedberg and T.D. Lee, Nucl. Phys. B202, 89, B210[FS6], 310,337 (1982).
4. T.W. Chiu, Phys. Lett. B 245 (1990) 570.
5. T.W. Chiu, Phys. Lett. B 217 (1989) 151.
6. T.W. Chiu, " Vacuum Polarization on the 4-D Random-Block Lattice ", California Institute of Technology preprint, $C^3P - 693$, 1989.